Physics and Imaging in Radiation Oncology 27 (2023) 100462

Contents lists available at ScienceDirect

Physics and Imaging in Radiation Oncology

journal homepage: www.sciencedirect.com/journal/physics-and-imaging-in-radiation-oncology

Original Research Article

An integrated and fast imaging quality assurance phantom for a 0.35 T magnetic resonance imaging linear accelerator

James J. Sohn, Sara Lim, Indra J. Das, Poonam Yadav *

Department of Radiation Oncology, Northwestern Memorial Hospital, Northwestern University Feinberg School of Medicine, IL 60611, USA

ARTICLE INFO

Keywords:
Magnetic resonance imaging linear accelerator
Imaging
Magnetic resonance imaging guided radiation therapy
MRIdian
QA
Magphan
ACR alternatives

ABSTRACT

Purpose: Periodic imaging quality assurance (QA) of magnetic resonance imaging linear accelerator (MRL) is critical. The feasibility of a new MRL imaging phantom used for QA in the low field was evaluated with automated image analysis of various parameters for accuracy and reproducibility.

Methods and materials: The new MRL imaging phantom was scanned across every 30 degrees of the gantry, having the on/off state of the linac in a low-field MRL system using three magnetic resonance imaging sequences: true fast imaging with steady-state precession (TrueFISP), T1 weighted (T1W), and T2 weighted (T2W). The DICOM files were used to calculate the imaging parameters: geometric distortion, uniformity, resolution, signal-to-noise ratio (SNR), and laser alignment. The point spread function (PSF) and edge spread function (ESF) were also calculated for resolution analysis.

Results: The phantom data showed a small standard deviation - and high consistency for each imaging parameter. The highest variability in data was observed with the true fast imaging sequence at the calibration angle, which was expected because of low resolution and short scan time (25 sec). The mean magnitude of the largest distortion measured within 200 mm diameter with TrueFISP was 0.31 ± 0.05 mm. The PSF, ESF, signal uniformity, and SNR measurements remained consistent. Laser alignment traditional offsets and angular deviation remained consistent.

Conclusions: The new MRL imaging phantom is reliable, reproducible, time effective, and easy to use for a 0.35 T MRL system. The results promise a more streamlined, time-saving, and error-free QA process for low-field MRL adapted in our clinical setting.

1. Introduction

The role of imaging in radiation therapy has become increasingly significant in recent years. A recent innovation has been the introduction of on-board real-time magnetic resonance imaging (MRI) guidance with hybrid magnetic resonance imaging linear accelerator (MRL) systems [1–2]. The MRL enables real-time tracking of tumors and surrounding organs at risk while delivering radiation beams. Magnetic resonance imaging guided radiation therapy (MRgRT) utilizes superior soft tissue contrast provided by MRI with treatment plan adaptation to perform an adaptive online radiotherapy treatment [3–6]. Globally, MRL installations have increased rapidly over the past few years. Currently, two vendors are offering MRgRT systems, Elekta Unity and ViewRay's MRIdian [1,7].

Since the 0.35 T ViewRay MRIdian MRL was first introduced in 2017, numerous papers have been published regarding MRL acceptance testing/commissioning and quality assurance (QA) [8–13]. Due to the presence of magnetic fields, the imaging QA of these MRL systems became critical to the accuracy of treatment delivery, such as MRI localization, voxel sizing, and distortion correction [14–15]. The American College of Radiology (ACR) requires periodic measurements in addition to manufacturer-recommended QA and diagnostic MRI accredited by the ACR, governing acceptance, commissioning, and other periodic QA on MRL [16]. Based on the American Association of Physicists in Medicine (AAPM) task group (TG)-233, ACR phantom- is used by physicists to evaluate key performance metrics of magnetic resonance (MR) scanners such as magnetic field homogeneity, geometric accuracy, slice thickness, low contrast detectability, high contrast spatial resolution, slice position accuracy, uniformity, radiofrequency coil checks, etc [17]. Although AAPM TG-284 addresses the needs and considerations

* Corresponding author at: Department of Radiation Oncology, Northwestern Memorial Hospital, Northwestern University Feinberg School of Medicine, Chicago, IL 60611, USA.
E-mail address: Poonam.yadav@nm.org (P. Yadav).

https://doi.org/10.1016/j.phro.2023.100462
Received 30 January 2023; Received in revised form 17 June 2023; Accepted 20 June 2023
Available online 22 June 2023

for QA of MRI simulation in radiotherapy with the ACR phantom, a dedicated QA procedure for radiation oncology still needs to be established and available since the MRL systems have recently been commercialized [18]. Additionally, it is well known that the imaging QA on MRL with the ACR phantom typically takes four hours, and the ACR test results require manual analysis, which is both time-consuming and tedious [19]. Thus, from the perspective of a clinical physicist, one option is to develop time-saving QA processes so that most of the imaging QA on MRL work can be automated. Other phantoms that may replace the ACR phantom for MRL are available to satisfy explicit expectations [20].

The Magphan RT phantom (The Phantom Laboratory, Salem, NY, USA) has been released, providing an integrated test that performs all measurements required to ensure MRI performance in MRgRT [21–23]. The phantom comes with a web-based software called "Smári" that allows comprehensive QA measurements for clinical MRI pulse sequences, accommodating various image types and contrast levels. It investigates failure mechanisms dependent on sequence, configuration, parameters, and operator, identifying issues before they escalate [23]. As MRL systems are still a relatively new development in Radiation Oncology, no papers have explored the utility of this phantom in low-field MRL as a periodic QA with clinical sequences. The purpose of this study is to investigate the alternatives to the ACR phantom for periodic QA and the clinical viability of a much-needed tool that is significant for both precision and saving time.

2. Methods and materials

2.1. Configuration of Magphan RT phantom

A ViewRay MRIdian system integrating a 0.35 T split bore MR scanner with a 6 MV flattening filter free linear accelerator was tested over time using Magphan. The Magphan® RT 820 phantom consists of two modules: the top module (TMR009) and the bottom module (TMR007). Fig. 1 illustrates the setup for periodic QA with the ACR phantom as well as the Magphan on MRL. With this two-piece configuration, the phantom can measure geometric distortion and uniformity over an area of $35 \times 27 \times 21$ cm^3. To evaluate the overall performance of the MRL, over 100 spherical fiducials and other components are filled with MRI-signal-generating liquid. The Magphan was filled meticulously to avoid bubbles. The phantom properties are not dependent on temperature but instead rely on the field strength and would be expected to be 175–225 ms at 0.35 T and 500–550 ms at 3.0 T. Several test objects and features are provided, including fiducial spheres for distortion measurements, three separate slice thickness ramps, three separate resolution apertures, noise rods for determining variation in non-signal

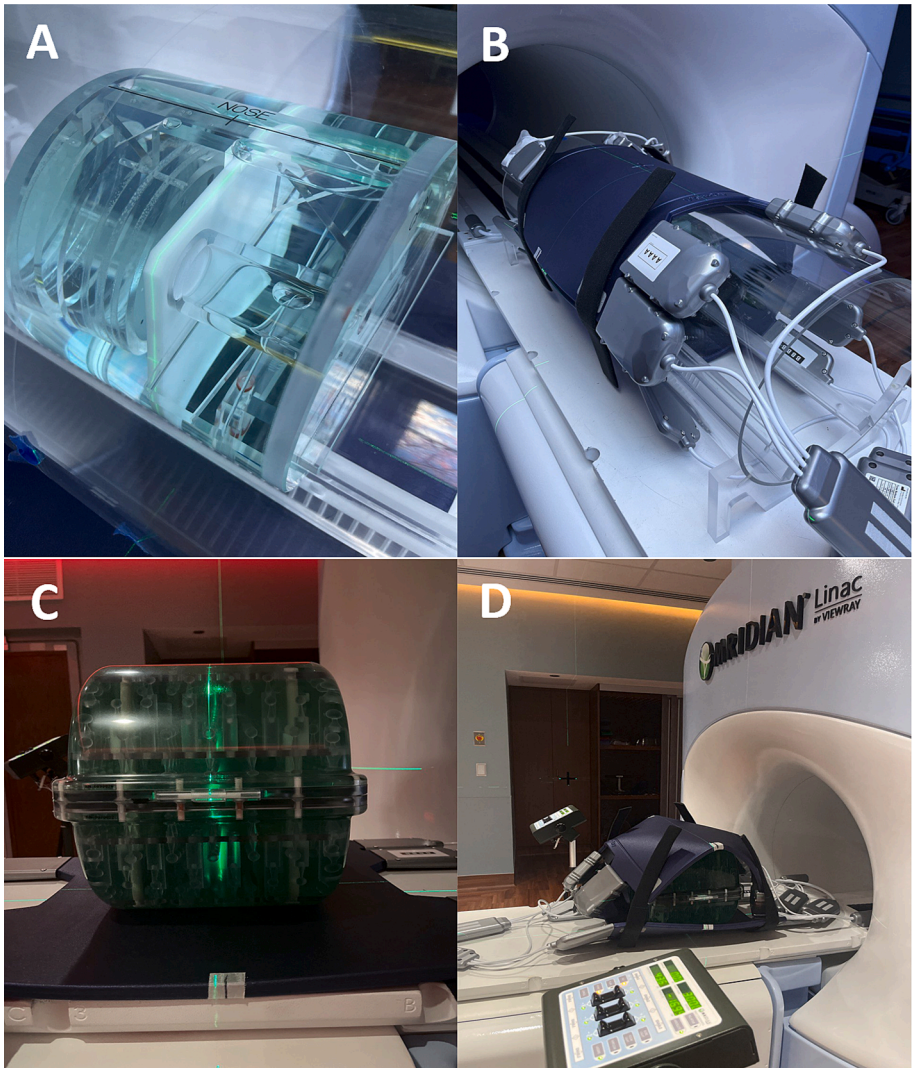

Fig. 1. Setup images for the ACR phantom without (A) and with (B) torso coils and the Magphan without (C) and with torso coils (D) for a periodic QA on the 0.35 T MR-Linac system.

areas, and uniform background fills to measure signal uniformity. Three separate ramps and apertures allow slice thickness and resolution measurements along any of the three cardinal axes.

2.2. Scanning and analyzing of Magphan RT phantom

The MRIdian system acquired three MR sequences, including true fast imaging with steady-state precession (TrueFISP), T1, and T2-weighted scans. It has two radiofrequency receiving coils equipped with preamplifiers for improved SNR. The Magphan phantom was scanned in an axial position at the isocenter between the torso coils. Various scan parameters were used and are summarized in supplementary material (Table S1).

Phantom was imaged at 30° intervals from 0° to 330° gantry angles and assessed the impact of gantry position on MRL imaging isocenter with linac mode on and off. To prevent artifacts, the treatment couch is deactivated during all RT mode image acquisitions. The scans were analyzed in detail, and the results were compiled into a comprehensive report by Smári. The ACR and Magphan data were compared to ensure optimal system performance. ACR phantom results were also collected and analyzed during the same period in order to compare the Magphan data. Although the ACR phantom's parameters are not identical to Magphan's, Table 1 provides a cross-comparison of the features of the ACR phantom, Magphan, and Insight phantom that Lewis et al [20] tested. With the torso coil on ViewRay MRIdian, all sequences were scanned with linac turned on and off at every 30 degrees of gantry angle. All data were analyzed from Smari except for T2-weighted (T2W) scans.

2.3. Measurements

2.3.1. Distortion

The Magphan measures distortion using spheres of diameter 1 cm as the primary fiducial marker. Fiducial markers in the Magphan are spaced approximately 4 cm apart. The mean magnitude of distortion was calculated. Fig. S1 in the supplementary material illustrates how the fiducials and other components are aligned on the Magphan.

2.3.2. SNR and slice thickness

The SNR is calculated for low-contrast detectability by dividing the average of the signal over a region near the center of the phantom by the standard deviation of the signal. The longitudinal tracking of SNR can provide early warning of degradation or failure of components. Using crossed ramps, a slice thickness is measured within a 1-mm thick slot carved out of solid plastic. Slice thickness is calculated based on the signal region's full width half maximum (FWHM) value. Crossed ramps compensate to first order for angular misalignment, and the final slice thickness is calculated using their geometry.

2.3.3. Resolution

Magphan measures the resolution of an MR system for high-contrast detectability using a circular aperture of 2 cm in diameter. The point spread function (PSF), modulation transfer function (MTF), and edge spread function (ESF) were calculated. The MTF is the magnitude of the Fourier Transform of the PSF that is a simple scalar characterization being the FWHM including low-contrast resolution. The ESF measures the spreading that would occur if an ideal step transition edge were imaged. A useful scalar characterization of the resolution is the width in mm required to transition from 10% to 90% of the step magnitude.

2.3.4. Signal uniformity

A three-dimensional uniformity measurement is performed using only background regions without any features, resulting in uniformity measurements over three dimensions. The normalized standard deviations (SDs) within a diameter were calculated by dividing by the mean of the signal in that diameter. In addition, the normalized spread was also calculated for signal uniformity, which is the difference in signal intensity between the mean of the 10% brightest voxels and the 10% dimmest voxels within either 200 mm or 350 mm diameter, divided by the mean of the signal within that diameter.

Table 1
Comparison list of tests that can be analyzed with the ACR phantom, the Insight phantom, and Magphan phantom.

	ACR phantom	Insight	Magphan
Geometric accuracy	Measure phantom diameter in four directions on the grid portion of the phantom (dia. = 190 mm)	Measure grid spacing in four directions including 200 mm horizontal, 200 mm vertical, 283 mm diagonals, and three peripheral regions 100 mm in length	Automated measurement of full 3D nonlinear distortion including 200 mm horizontal, 200 mm vertical, and 200 mm diagonal with a tolerance of less than 0.2 mm
High contrast spatial resolution	Frequency and phase encoding direction resolution hole array pairs	–	Automated measurement of system response functions - ESF, PSF, MTF. Quantitative output of characteristic widths such as 10–90% transition width of ESF
Periodic spatial resolution	–	Modulation transfer function calculation within 7.5 cm^2 circular ROIs drawn over frequency and phase encoding specific line pairs	Automated measurement of MTF in any three cardinal scan planes
Slice thickness accuracy	One pair of signal ramps	Five pairs of signal ramps	Three pairs of signal ramps aligned along cardinal axes
Slice position accuracy	Using separation of the two edges of a 45° wedge pair	–	Incorporated into 3D distortion analysis
Setup position accuracy	–	Four sets of plane alignment structures with 1.5 mm and 3.0 mm channels	Laser alignment features and automated analysis of translational and rotational phantom placement relative to MR system
Image intensity uniformity	Percent integral uniformity from high- and low-intensity regions of a large uniformity region	Uniformity expressed as the average of standard deviations from four 15 cm^2 circular ROIs	3D measurement of signal uniformity, expressed as normalized standard deviation and normalized 'spread' (difference between brightest and dimmest voxels)

*SNR: signal-to-noise ratio, ESF: edge spread function, PSF: point-spread function, MTF: modulation transfer function, ROI: region-of-interest, MR: magnetic resonance.

2.3.5. Laser alignment

Phantom placement tests are performed to monitor the alignment between the MR system isocenter and the laser system. According to the analysis, the offset of all three cardinal axes from the isocenter of the MR system can be determined in terms of translational and rotational displacement.

3. Results

This study shows that there is no difference between having the linac on or off in terms of impact/difference. Based on the results, the magnetic field was shimmed correctly at all gantry angles.

3.1. Distortion

Fig. 2 shows the geometric accuracy of 200 mm (A and C) and 350 mm (B and D) in diameter from the isocenter. The upper two represent the mean of the magnitude of the distortion of the 10% most distorted measurements. The maximum geometric error within the 200 mm diameter was 0.38 mm, occurring in the gantry 240° with the linac off on the 25 s planning scan. The mean magnitude of the largest distortion measured within 200 mm diameter with TrueFISP was 0.31 ± 0.05 mm. The maximum geometric error within the 350 mm diameter was 0.92 mm, occurring in the gantry 300° with the linac off on the T2W scan. The mean magnitude of the largest distortion measured within 350 mm diameter with TrueFISP was 0.99 ± 0.10 mm.

3.2. SNR and slice thickness

The mean SNR values on TrueFISP, T1W, and T2W were 36.46 ± 13.21, 31.72 ± 1.40, and 15.52 ± 5.59, respectively. The SNR in overall gantry angles were homogeneous and T2W has the lowest SNR values as seen in Fig. 3 A. The slice thickness was derived on the 172 s planning scan only (Fig. 3 B), which is TrueFISP that has a slice thickness of 1.5 mm, the mean and SD was 2.40 ± 0.08 mm. Although a few data were derived for the slice thickness measurements on T1W, with the slice thickness of 1.5 mm, however, the mean and SD were 5.87 ± 1.99 mm.

3.3. Resolution

For ESF 10% to 90% of the transition widths, the mean and SD values on TrueFISP, T1W, and T2W were 1.83 ± 0.12 mm, 2.42 ± 0.06 mm, and 2.44 ± 0.13 mm, respectively, as shown in Fig. 4 A. For PSF on horizontal and vertical FWHMs (Fig. 4 B), the mean and SD values on TrueFISP, T1W, and T2W were 2.21 ± 0.10 mm, 2.79 ± 0.04 mm, and 2.44 ± 0.10 mm, respectively.

3.4. Signal uniformity

The signals from all sequences were uniform across all gantry angles, as shown in Fig. 5. Within the 200 mm (Fig. 5 A and C) diameter, the mean and SD values on TrueFISP, T1W, and T2W were 297.98 ± 73.12, 533.62 ± 4.83, and 232.27 ± 22.37, respectively. Within the 350 mm (Fig. 5 B and D) diameter, the mean and SD values on TrueFISP, T1W, and T2W were 364.80 ± 78.32, 617.29 ± 10.36, and 265.60 ± 27.25, respectively.

3.5. Laser alignment

The phantom alignment has been analyzed as a six degree-of-freedom (6DoF). The overall mean and SD values translation shift with all sequences for the right-left (R-L), anterior-posterior (A-P), and superior-inferior (S-I) were 0.6 ± 0.44 mm, −0.32 ± 0.83 mm, and −0.44 ± 1.44 mm, respectively. The overall mean and SD values rotational shift with all sequences for the yaw, pitch, and roll was 0.0 ± 0.11

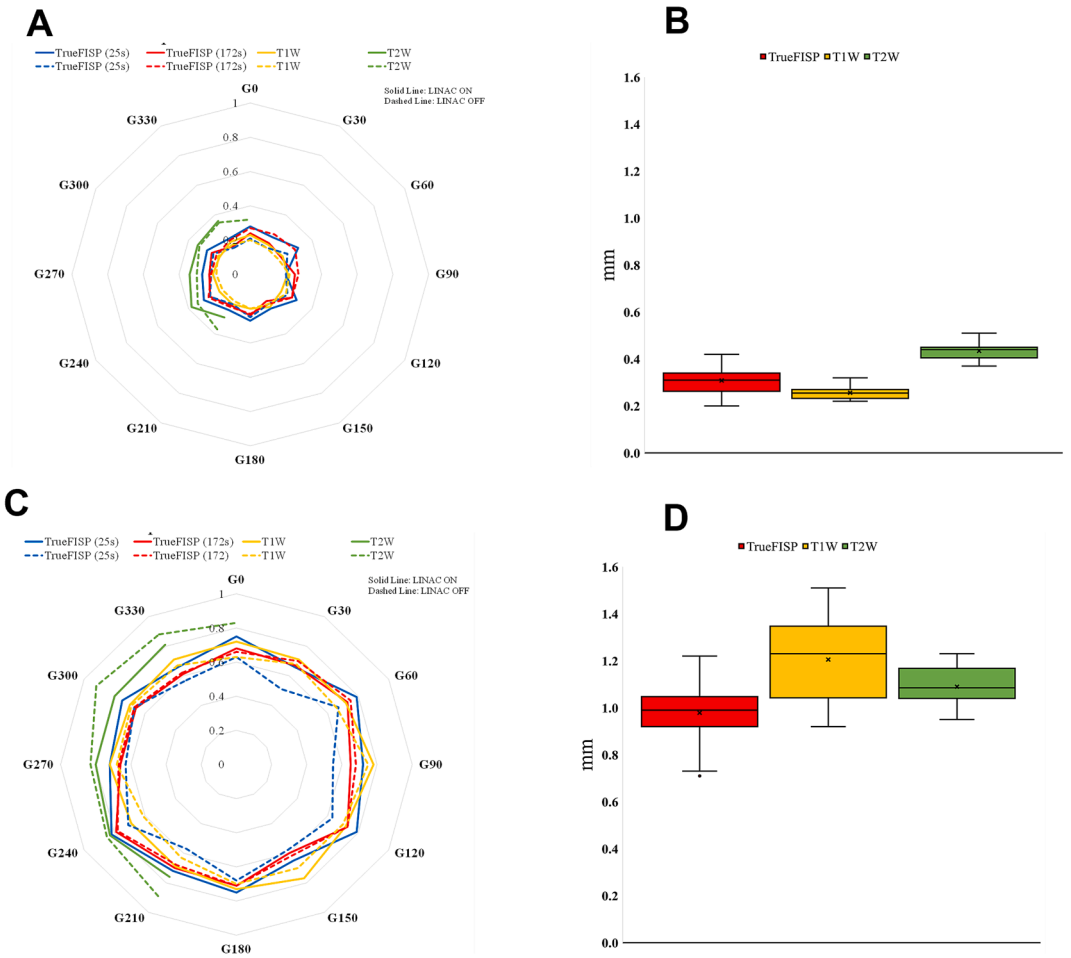

Fig. 2. The RT distortion from all MR sequences on 0.35 T MR-linac with the Magphan within (A and B) 200 mm and (C and D) 350 mm diameter across all gantry angles. Data is presented in polar representation in A and C and overall analysis of the same data is shown in B and D.

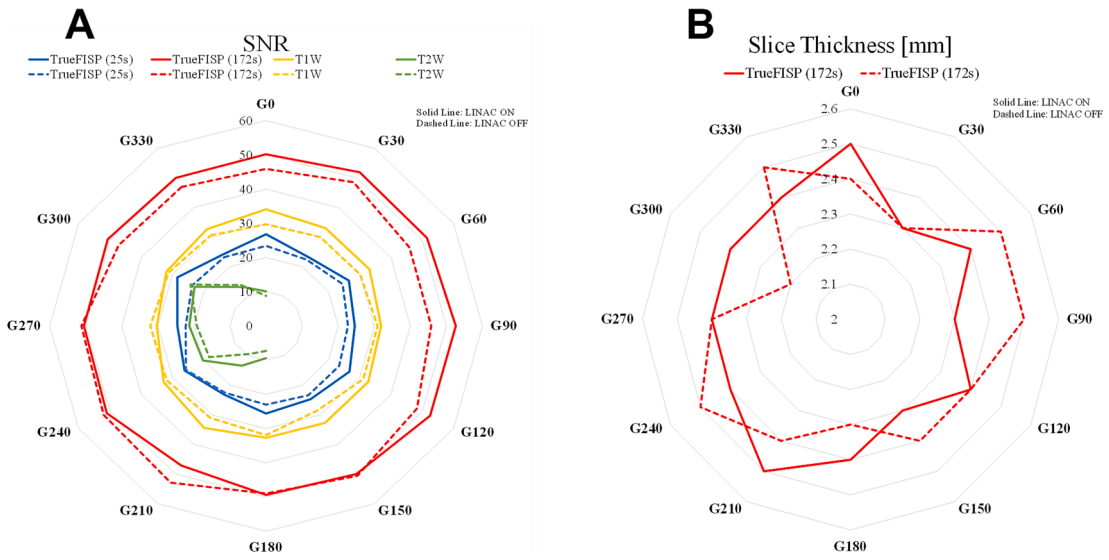

Fig. 3. The SNR for all MR sequences on 0.35 T MR-linac are shown in A and slice thickness for True FISP scan is plotted in B.

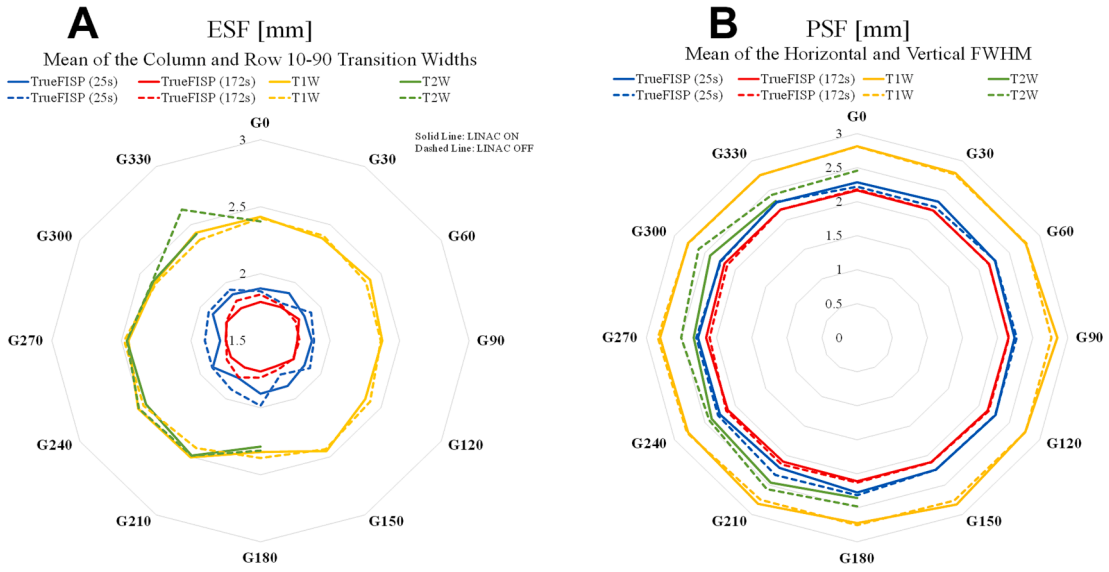

Fig. 4. The resolution across the all-gantry angles from all MR sequences on 0.35 T MR linac with the Magphan. (A): the mean of both column and row 10%–90% step magnitude for the ESF is shown and in (B): the PSF, all other resolution measurements were derived, including low-contrast resolution.

mm, 0.52 ± 0.48 mm, and −0.23 ± 0.05 mm, respectively and the details can be seen in the supplementary material S2.

4. Discussion

Magphan provides a complete and convenient QA methodology for monitoring all performance parameters of an MR scanner, providing extensive FOV coverage in an easy-to-handle and completely automated analysis. For scans with sufficiently high SNRs this can be a reliable measurement. For scans with lower SNRs, and where isotropic resolution is expected, it can be advantageous to calculate isotropic MTF, PSF, and ESF functions. As the gantry moves, the phantom placement can disturb the scanner's magnetic field, causing an apparent shift in the MR coordinate system. This is an effect of the large mass of metal in the gantry rather than the on/off state of the linac. Latifi et al. [24] studied the effect and compared the Magphan to another phantom for measuring apparent shifts in the MR coordinate origin. The T2-weighted images contain some artifacts that prevent the distortion analysis from running because some spheres are missing. A lower sphere detection threshold parameter can be set in the Smari for analysis. This could cause errors in the measurement, mainly if the missing spheres cause a large region of space not to be measured. Laser traces appear differently due to disturbances in the magnetic field affecting different directions in different ways. The results of the laser indicate that the phase encoding direction is A-P, since shifts in the magnetic field have a larger impact on the frequency encode direction than the phase encode direction. The misalignments in the translation shifts for the same condition (i.e., gantry 300°with the TureFISP 172 s sequence) were from 1.3 to 0.8 for the R-L, from −1.1 to −1.6 for the A-P, and from −2.1 to −1.7 for the S-I. The misalignments in the rotational shifts for the same condition (i.e., gantry 300° with the TureFISP 172 s sequence) were from 0.1 to −0.2 for the yaw, from 0.1 to 0 for the pitch, and from −0.3 to −0.1 for the roll. Particularly, the rotational shifts agreed with our machine's inherent and known-values, however, the translational shifts were not derived as expected. We concluded that it is difficult to align the Magphan perfectly since the oval shape of the Magphan design causes it to be physically

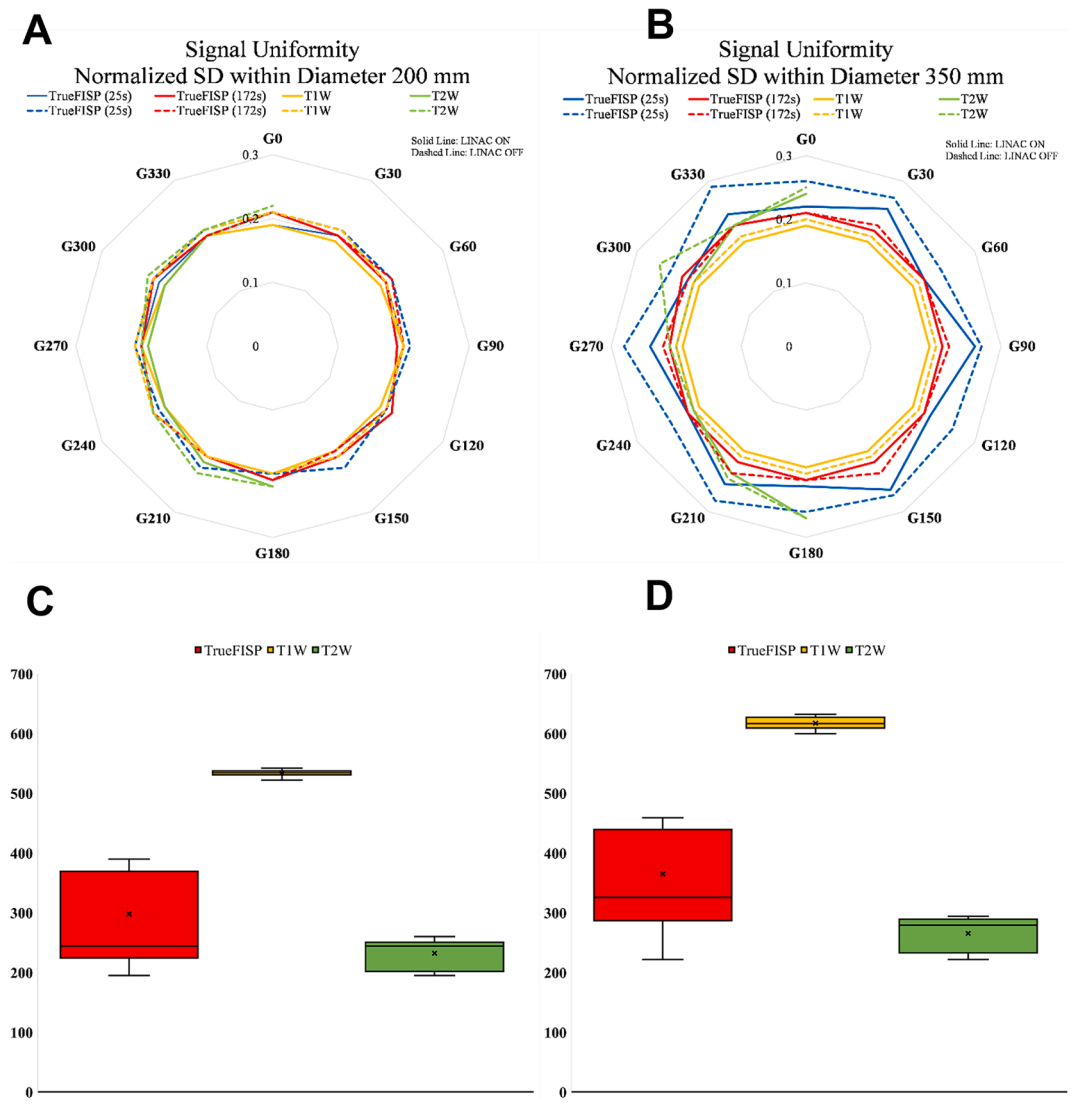

Fig. 5. The signal uniformities with the normalized SD from all MR sequences on MR linac with the Magphan within 200 (A and C) mm and 350 mm (B and D) diameter. The normalized SD represents the signal within the diameter divided by the mean of the signal in that diameter.

tilted when wrapped around the torso coils.

MRgRT-based radiotherapy treatment planning requires limiting distortions in MR scans. For 1.5 T MRL, Tijssen et al [8] characterized the distortions due to scanner-related distortions using vendor-specific distortion correction algorithms. A QA must also ensure that the corrections applied are robust. As ACR tests do not cover this aspect of distortions, treatment planning may be adversely affected. The maximum distortion allowed for ACR accreditation of MR programs is ±2 mm, and the distortion should not exceed 2% when the images are used for treatment planning. For T1-weighted images, distortion was measured at less than 0.4 mm with Magphan. As recommended by the manufacturer, Dorsch et al. showed distortion tolerances of 1 mm and 2 mm for their phantom [25].

There is limited literature on using Magphan RT phantom in low-field MRL. Ericsson-Szencsenyi examined radiomics features with the ViewRay system and Magphan's QA images. Dorch et al suggested a custom PMMA phantom for isocenter alignment and image distortion [25]. Gach et al found that Magphan can be used for B0 field homogeneity in Elekta's Unity MRL (1.5 T) but did not consider onboard MRI QA with a low field MRL (0.35 T).

In general, QA may help in proactively finding issues with the system, thereby reducing system downtime. As the existing monthly QA tests are done in MR-only mode (while the linac is off), it is imperative that integrated testing be implemented for the simultaneous use of the MR scanner and the linac in clinical mode. Studies have suggested exploring dedicated setup and QA procedures during gated delivery. As a result of our approach of testing the system in clinical mode, we are able to assess the system's reliability for online adaptive radiotherapy workflows. Clinics vary in the types of tools they use to analyze ACR results, and often they use in-house tools or other custom-tailored tools. Therefore, the probability of manual errors is higher compared to the use of automated analysis tools. Using Magphan and its Smari software, the result analysis is not only quick and fully automated, but also establishes a uniformly standardized analysis platform, alleviating local testing challenges. An example of Smari's analysis can be seen in the supplementary material S3.

There are a few limitations to the QA apparatus used in our study. Slice thickness should not exceed 3 mm, and SNR should be sufficient for analyses. Some T2-weighted images may not meet these requirements and cannot be analyzed automatically. Measuring slice thickness of thin slices requires high SNR, and for this sequence, the slice thickness measurement in the Magphan has a variability of approximately ±0.2 mm. Therefore, within the uncertainty in the measurement, there is no discernible difference between the slice thickness measurements with the Linac on vs Linac off. The agreement between the gantry angles when performing QA for slice thickness could be due to a number of

factors, including shimming alignment, positioning, or software. If shimming is an issue, additional shimming may be necessary. In order to determine the root cause of the poor agreement between the gantry angles, it may be necessary to perform a more comprehensive QA assessment, including evaluating the mechanical alignment of the scanner, the gantry positioning, and the software parameters. The presence of artifacts may impact Magphan's ability to calculate slice thickness, but this is primarily a problem with T2-weighted images. The Magphan analysis is not affected by phantom positioning, but the ACR phantom is sensitive and could impact results. Distortion measurements are only possible in areas with fiducials. Without fiducials, precise placement is not necessary for the Magphan. However, the Magphan does not offer signal ghosting tests at higher levels than what is typically seen in functioning scanners. A B0 test is also not provided. Automated analysis can reduce analysis time from 40 to 5 min, saving significant workload and improving throughput. The Magphan approach provides a more efficient and reliable QA program, with setup and analysis completed in just 20 min. It offers at least six parameters and can provide sophisticated 3D measurements with only a single pulse sequence. Unlike the ACR phantom, there is no subjectivity involved in the analysis. Magphan is a practical and valuable tool for describing the performance of a low-field MRL and monitoring it over time. In conclusion Magphan is an excellent alternative to the ACR phantom for evaluating low-field MRL performance. It's faster to use and has similar measurements. However, keeping the ACR phantom as a backup for occasional analysis is still advisable.

Funding

None.

Declaration of Competing Interest

The authors declare that they have no known competing financial interests or personal relationships that could have appeared to influence the work reported in this paper.

Acknowledgments

The authors gratefully acknowledge Dr. Richard Mallozzi, Phantom Laboratory, Inc., who kindly shared his expertise and the time to explain more details from the Smari.

Appendix A. Supplementary data

Supplementary data to this article can be found online at https://doi.org/10.1016/j.phro.2023.100462.

References

[1] Kerkmeijer LG, Fuller CD, Verkooijen HM, Verheij M, Choudhury A, Harrington KJ, et al. The MRI-linear accelerator consortium: evidence-based clinical introduction of an innovation in radiation oncology connecting researchers, methodology, data collection, quality assurance, and technical development. Phys Imaging Radiat 2016;6:215. https://doi.org/10.1016/j.phro.2016.10.007.

[2] Das IJ, Yadav P, Mittal BB. Emergence of MR-Linac in radiation oncology: successes and challenges of riding on the MRgRT bandwagon. J Clin Med 2022;11:5136. https://doi.org/10.3390/jcm11105136.

[3] Klüter S. Technical design and concept of a 0.35 T MR-Linac. Phys Imaging Radiat 2019;18:98–101. https://doi.org/10.1016/j.phro.2019.07.008.

[4] Mutic S, Low D, Chmielewski T, Fought G, Gerganov G, Hernandez M, et al. The design and implementation of a novel compact linear accelerator–based magnetic resonance imaging–guided radiation therapy (MR-IGRT) system. Phys Imaging Radiat 2016;96:E641. https://doi.org/10.1016/j.ijrobp.2016.07.006.

[5] Deshmane A, Gulani V, Griswold MA, Seiberlich N. Parallel MR imaging. Phys Imaging Radiat 2012;36:55–72. https://doi.org/10.1016/j.mri.2017.02.020.

[6] Metcalfe P, Liney G, Holloway L, Walker A, Barton M, Delaney G, et al. The potential for an enhanced role for MRI in radiation-therapy treatment planning. Technol Cancer Res Treat 2013;12:429–46. https://doi.org/10.7785/tcrt.2012.500364.

[7] Hall WA, Paulson E, Li XA, Erickson B, Schultz C, Tree A, et al. Magnetic resonance linear accelerator technology and adaptive radiation therapy: an overview for clinicians. CA Cancer J Clin 2022;72:34–56. https://doi.org/10.3322/caac.21633.

[8] Tijssen RH, Philippens ME, Paulson ES, Glitzner M, Chugh B, Wetscherek A, et al. MRI commissioning of 1.5 T MR-linac systems–a multi-institutional study. Radiother Oncol 2019;132:114–20. https://doi.org/10.1016/j.radonc.2018.12.002.

[9] Snyder JE, St-Aubin J, Yaddanapudi S, Boczkowski A, Dunkerley DA, Graves SA, et al. Commissioning of a 1.5 T Elekta Unity MR-linac: a single institution experience. J Appl Clin Med Phys 2020;21:160–72. https://doi.org/10.1002/acm2.12829.

[10] Roberts DA, Sandin C, Vesanen PT, Lee H, Hanson IM, Nill S, et al. Machine QA for the Elekta Unity system: a report from the Elekta MR-linac consortium. Med Phys 2021;48:e67–85. https://doi.org/10.1002/mp.14923.

[11] Price AT, Knutson NC, Kim T, Green OL. Commissioning a secondary dose calculation software for a 0.35 T MR-linac. J Appl Clin Med Phys 2022;23:e13452. https://doi.org/10.1002/acm2.13452.

[12] Stanescu T, Tadic T, Jaffray DA. Commissioning of an MR-guided radiation therapy system. Int J Radiat Oncol Biol Phys 2014;90:S94–5. https://doi.org/10.1016/j.ijrobp.2014.05.234.

[13] Khan AU, DeWerd LA, Das IJ, Yadav P. A multi-institutional comparison of acceptance testing data for a 0.35 T MRI scanner. Phys Med Biol 2022;67:05NT01. https://doi.org/10.1088/1361-6560/ac2166.

[14] Das IJ, McGee KP, Tyagi N, Wang H. Role and future of MRI in radiation oncology. Br J Radiol 2019;92:20180505. https://doi.org/10.1259/bjr.20180505.

[15] Cao Y, Tseng CL, Balter JM, Teng F, Parmar HA, Sahgal A. MR-guided radiation therapy: transformative technology and its role in the central nervous system. Neuro Oncol 2017;19:ii16–29. https://doi.org/10.1093/neuonc/nox090.

[16] Christiansen RL, Dysager L, Bertelsen AS, Hansen O, Brink C, Bernchou U. Accuracy of automatic deformable structure propagation for high-field MRI guided prostate radiotherapy. Radiat Oncol 2020;15:1–11. https://doi.org/10.1186/s13014-020-01595-0.

[17] Huq MS, Fraass BA, Dunscombe PB, Gibbons JP, Ibbott GS, Mundt AJ, et al. The report of Task Group 100 of the AAPM: Application of risk analysis methods to radiation therapy quality management. Med Phys 2016;43:4209–62. https://doi.org/10.1118/1.4949382.

[18] Glide-Hurst CK, Paulson ES, McGee K, Tyagi N, Hu Y, Balter J, et al. Task group 284 report: magnetic resonance imaging simulation in radiotherapy: considerations for clinical implementation, optimization, and quality assurance. Med Phys 2021;48:e636–70. https://doi.org/10.1002/mp.14680.

[19] Wetscherek A, van der Bijl E, van Lier AL, Chick J, Jackson S, Gibson S, et al. Longitudinal stability of MRI QA up to two years on eight clinical 1.5 T MR-Linacs. Front Phys 2022;5:26. https://doi.org/10.3389/fphy.2022.00026.

[20] Lewis BC, Shin J, Maraghechi B, Quinn B, Cole M, Barberi E, et al. Assessment of a novel commercial large field of view phantom for comprehensive MR imaging quality assurance of a 0.35 T MRgRT system. J Appl Clin Med Phys 2022;23:e13535. https://doi.org/10.1002/acm2.13535.

[21] Ericsson-Szecsenyi R, Zhang G, Redler G, Feygelman V, Rosenberg S, Latifi K, et al. Robustness assessment of images from a 0.35 T scanner of an integrated MRI-Linac: characterization of radiomics features in phantom and patient data. Technol Cancer Res Treat 2022;21. https://doi.org/10.1177/15330338221099113. 15330338221099113.

[22] Ericsson-Szecsenyi R. Characterization of Radiomics Features Extracted from Images Generated by the 0.35 T Scanner of an Integrated MRI-Linac. 2020. [Thesis].

[23] Walker A, Chlap P, Causer T, Mahmood F, Buckley J, Holloway L. Development of a vendor-neutral MRI distortion quality assurance workflow. J Appl Clin Med Phys 2022;23:e13735.

[24] Latifi K, Moros EG, Zhang G, Harrison L, Feygelman V. A method to determine the coincidence of MRI-guided linac radiation and magnetic isocenters. Technol Cancer Res Treat 2019;18. https://doi.org/10.1177/1533033819877986. 1533033819877986.

[25] Dorsch S, Mann P, Elter A, Runz A, Spindeldreier C, Klüter S, et al. Measurement of isocenter alignment accuracy and image distortion of an 0.35 T MR-Linac system. Phys Med Biol 2019;64:205011. https://doi.org/10.1088/1361-6560/ab4c27.